

Implicit and Explicit Numerical Integration Schemes Applied to Elastoplastic Constitutive Laws for Soils

D.M. Pedroso and M.M. Farias

Post-graduation Program in Geotechnics, University of Brasilia, Brazil

ABSTRACT: The constitutive relation of elastoplastic materials generates a Differential Algebraic System (DAS), which is generally solved numerically. The solution of this system in the context of Finite Elements is called Stress-Point Integration. Different integration schemes are available and their accuracy and efficiency should be investigated for each constitutive model. These schemes are generally divided into implicit and explicit. Among the explicit schemes, the most used are the Forward-Euler (FE) and the Modified-Euler (ME). Among the implicit schemes, the fully implicit or Backward-Euler (BE) is widely used. The Backward Euler scheme solves the DAS simultaneously updating stress and internal variables, at the same time that consistency is guaranteed. In this paper the Modified-Euler scheme is used with an algorithm, which automatically subdivides the imposed strain increments, keeping the truncation error within a prescribed tolerance. Here BE and ME schemes are applied to the integration of the constitutive relations of two subloading models, named Sub-Cam and Sub-tij, for a wide range of imposed strain increments and initial stress conditions. The solutions are compared with the “exact” solution obtained with the FE scheme with very small strain increments. The results show that the Backward-Euler scheme takes a great number of small increments to converge to the correct solution. Overall the Modified Euler scheme with automatic step algorithm gives the most accurate results at a lower computational cost.

1 INTRODUCTION

According to the continuum mechanics theory, the application of external loads to any continuum mass of soil causes changes in stress and strains. This theory establishes basic concepts, such as stress and strain, that allows for the study of the internal response of the soil mass for given boundary conditions. A key concept regarding the solution of this *Initial Boundary Value Problem* is the *Constitutive Law* (or model) that relates stress to strain at each point inside a body.

Nakai & Hinokio (2004) proposed the Subloading tij model (Sub-tij for short) that is very efficient to represent soil materials subject to cyclic loads. This model is based on the concept of *Subloading* first introduced by Hashiguchi & Ueno (1977) and on the tij-Clay and tij-Sand models introduced by Nakai & Matsuoka (1986) and Nakai (1989), respectively. These series of elastoplastic models are based on the Cam Clay model (Desai & Siriwardane, 1984). Here, an extended version of the Cam Clay model, named Subloading Cam-clay (Sub-Cam for short), will be proposed mainly to help check integration algorithms.

Non-linear constitutive laws are given by rate equations. Therefore, some way to integrate these equations is required. Since analytical solutions are generally difficult to be found, numerical schemes are adopted. The constitutive relation of elastoplastic materials constitutes a *Differential Algebraic System (DAS)* (Buttner & Simeon, 2002). The solution of this system in the context of Finite Elements is called *Stress-Point Integration* and the constitutive laws must be integrated for finite increments of strain (Simo & Hughes, 1998).

Many integration schemes are available. Since for the FEM codes, speed is always important, the efficiency of any stress-point integrator should be investigated. This is also important considering the specific constitutive model adopted. Another very important study is the accuracy of the integration scheme when solving the DAS for different constitutive laws. These schemes are generally divided into implicit and explicit, according to the time-position at which the gradients are evaluated. Among the explicit schemes, the most used are the *Forward-Euler (FE)* and

the *Modified-Euler (ME)*. Among the implicit schemes, the fully implicit or *Backward-Euler (BE)* is widely used.

It is important to solve all equations of elastoplastic DAS at the same time during the stress-point integration. This implies that both the constitutive law equations and evolution equations for the internal variables should be integrated using the same scheme. The Modified-Euler scheme presented here, based on the one given by Sloan et al. (2001), take this in consideration.

In this paper, according to Sloan (1987), Sloan & Booker (1992) and Sloan et al. (2001), the Modified-Euler (ME) scheme is used with an algorithm, which automatically subdivides the imposed strain increments, keeping the truncation error within a prescribed tolerance. The Fully Backward Euler (BE) scheme solves the DAS simultaneously updating stress increments and internal variables, at the same time that consistency is guaranteed. Here BE and ME schemes are applied to the integration of the constitutive relations of the subloading models: Sub-Cam and Sub-tij, for a wide range of imposed strain increments and initial stress conditions.

The range of strain increments is chosen according to a virtual grid made of $\Delta\varepsilon_1 \times \Delta\varepsilon_2$ points. These values are selected in such a way that the corresponding final stress states increases in both deviatoric and volumetric states, i.e, moving away from the yield surface. The initial stress states studied are positioned at different combinations of mean and shear stress. For each grid of given strain increments, isoerror lines like the ones showed in Simo & Hughes (1998) are plotted to help the study of the accuracy. The solutions of each scheme are compared to the “exact” solution obtained with the FE scheme with a large number of sub-divisions of the increments that corresponds to very small strain increments.

2 ELASTOPLASTIC MODELS

Elastoplastic models are formulated as rate or infinitesimal incremental relations between stress and strain tensors. These relations form a Differential Algebraic System (DAS) subject to some Kuhn-Tucker restrictions. The first step in developing these models is the assumption of linear

decomposition of the strain increment (rate) into an elastic and a plastic tensor. From the generalised Hooke's law the following basic equation is obtained:

$$\dot{\underline{\underline{\boldsymbol{\sigma}}}} = \underline{\underline{\underline{\underline{D}}}}^e : \left(\dot{\underline{\underline{\boldsymbol{\varepsilon}}}} - \dot{\underline{\underline{\boldsymbol{\varepsilon}}}}^p \right) \quad (1)$$

in which $\dot{\underline{\underline{\boldsymbol{\sigma}}}}$ is the second order stress rate tensor, $\dot{\underline{\underline{\boldsymbol{\varepsilon}}}}$ is the second order total strain rate tensor, $\dot{\underline{\underline{\boldsymbol{\varepsilon}}}}^p$ is the second order plastic strain rate tensor and $\underline{\underline{\underline{\underline{D}}}}^e$ is the fourth order elastic rigidity moduli tensor. The notation and operations used in this paper are defined in Appendix A.

Besides the stress-strain evolution, it is also considered the existence of a set of stress-like z_i and strain-like ξ_i *internal variables*, related to plastic hardening (Simo, 1994). The evolution of these internal variables is linked by a series of *hardening rigidity moduli* H_i as follows:

$$\dot{z}_i = H_i \dot{\xi}_i \quad (\text{no sum on } i) \quad (2)$$

Eqs. (1) and (2) form the basic relations for any elastoplastic model. Specific models will differ on adopted functions for the yield surface, plastic potential surface and hardening law. The yield function $f(\underline{\underline{\boldsymbol{\sigma}}}, z_i)$ sets a limit in the stress space for the occurrence of plastic strains. The plastic potential function gives the direction of plastic flow $\dot{\underline{\underline{\boldsymbol{\varepsilon}}}}^p$. The hardening law establishes the internal variables of the model and how they relate.

For a generic elastoplastic model the flow rule is obtained by defining a second order tensor $\underline{\underline{\boldsymbol{r}}}$ that gives the direction of plastic flow. Thus

$$\dot{\underline{\underline{\boldsymbol{\varepsilon}}}}^p = \dot{\Lambda} \underline{\underline{\boldsymbol{r}}} \quad (3)$$

in which $\dot{\Lambda}$ is a scalar plastic multiplier, obtained by imposing the consistency condition $\dot{f} = 0$.

The elastoplastic models used in this paper consider the concept of "subloading", originally proposed by Hashiguchi & Ueno (1977). According to this concept, two yield surfaces are necessary: the first one is used to smooth the elastic-plastic transition and the second one is the usual surface used to memorise the maximum plastic state to which the point was subjected. The first surface is called *subloading surface* and the stress point always lies on it. The second surface is called *normal yield surface* and encapsulates the subloading surface, coinciding with it only if the point is normally consolidated.

When using subloading models it is necessary to define separate internal variables and evolution laws for the two surfaces. The actual stress point always lies on the subloading surface, therefore both consistency and flow rule are imposed on this surface. The internal variables of the normal yield surface affect the hardening modulus of the subloading surface, thus linking both surfaces.

Hereafter, the internal variables related to the subloading surface will be denoted by an array z_α and ξ_α , while those related to the normal surface will be denoted by z_β and ξ_β , in which α and β are indexes ranging from one to the number of internal variables related to the subloading surface and from one to the number of internal variables related to the normal surface, respectively.

The strain-like internal variables are defined as scalar functions of the plastic (rate) strain tensor through the Lagrange multiplier. Therefore, the following hardening laws may be written

$$\dot{\xi}_\alpha = \dot{\Lambda} h_\alpha \quad \text{and} \quad \dot{\xi}_\beta = \dot{\Lambda} h_\beta \quad (4)$$

in which h_α and h_β are scalar functions that define the type of hardening rule used in the model.

Substituting Eq. (1) and Eq. (3) into the consistency condition, the Lagrangian multiplier can be expressed as:

$$\dot{\Lambda} = \frac{1}{\Phi} \underline{\underline{\boldsymbol{v}}} : \underline{\underline{\underline{\underline{D}}}}^e : \dot{\underline{\underline{\boldsymbol{\varepsilon}}}} = \underline{\underline{\boldsymbol{b}}} : \dot{\underline{\underline{\boldsymbol{\varepsilon}}}} \quad \left(\underline{\underline{\boldsymbol{b}}} = \frac{1}{\Phi} \underline{\underline{\boldsymbol{v}}} : \underline{\underline{\underline{\underline{D}}}}^e \right) \quad (5)$$

where the following variables were defined

$$\Phi = \underline{\underline{\boldsymbol{v}}} : \underline{\underline{\underline{\underline{D}}}}^e : \underline{\underline{\boldsymbol{r}}} - \sum_\alpha y_\alpha \mathcal{H}_\alpha \quad (6)$$

$$\underline{\underline{\boldsymbol{v}}} = \frac{\partial f}{\partial \underline{\underline{\boldsymbol{\sigma}}}} \quad (7)$$

$$y_\alpha = \frac{\partial f}{\partial z_\alpha} \quad (8)$$

$$\mathcal{H}_\alpha = H_\alpha h_\alpha \quad (\text{no sum on } \alpha) \quad (9)$$

Substituting Eq. (5) into Eq. (3) and the resulting expression into Eq. (1), one finds the stress-strain evolution law as:

$$\dot{\underline{\underline{\boldsymbol{\sigma}}}} = \underline{\underline{\underline{\underline{D}}}}^{ep} : \dot{\underline{\underline{\boldsymbol{\varepsilon}}}} \quad (10)$$

in which the fourth order elastoplastic rigidity tensor is computed as:

$$\underline{\underline{\underline{\underline{D}}}}^{ep} = \underline{\underline{\underline{\underline{D}}}}^e - \frac{1}{\Phi} \left(\underline{\underline{\underline{\underline{D}}}}^e : \underline{\underline{\boldsymbol{r}}} \right) \otimes \left(\underline{\underline{\boldsymbol{v}}} : \underline{\underline{\underline{\underline{D}}}}^e \right) \quad (11)$$

Furthermore, substituting Eq. (5) into Eq. (4) and the resulting expression into Eq. (2), one finds the expression for the evolution law for the internal stress-like:

$$\dot{z}_i = \mathcal{H}_i \underline{\underline{\boldsymbol{b}}} : \dot{\underline{\underline{\boldsymbol{\varepsilon}}}} \quad (12)$$

Eqs. (10) and (12) form the Differential Algebraic System (DAS) of the model and both have to be satisfied simultaneously for a given strain (or stress) increment. The particular expression for a given model depends basically on the suitable definitions of a yield function $f(\underline{\underline{\boldsymbol{\sigma}}}, z_i)$, on the direction of plastic flow $\underline{\underline{\boldsymbol{r}}}$ and on the choice of (internal) hardening variables and hardening rule. These are detailed for two models studied in this paper in the next sub-items.

2.1 Subloading Cam-clay

The Subloading Cam clay model, or Sub-Cam for short, is defined here as a simple extension of the modified Cam-clay model (Desai & Siriwardane, 1984), into which the subloading concept is introduced in the same way as presented by Nakai & Hinokio (2004). The subloading surface of Sub-Cam model is assumed to have the same expression as for the modified Cam clay model:

$$f(\underline{\underline{\boldsymbol{\sigma}}}, z_\alpha) = M^2 p (p - z_\alpha) + q^2 \quad (13)$$

in which p and q are the mean and deviatoric stress invariants, respectively, and z_α (the stress-like internal hardening variable) represents p_1 , i.e., the maximum mean stress ever imposed to the point. M is a model parameter related to the friction angle at critical state at compression ϕ_{CS} , and given by

$$M = \frac{6 \sin \phi_{CS}}{3 - \sin \phi_{CS}} \quad (14)$$

As for modified Cam clay, an associated flow rule is also assumed. Therefore the plastic flow direction is given by the normal to the subloading yield surface:

$$\underline{\underline{\boldsymbol{r}}} = \frac{df}{d\underline{\underline{\boldsymbol{\sigma}}}} \quad (15)$$

An expression similar to Eq. (13) could be written for the normal yield surface, by substituting the stress point

by its image $\underline{\sigma}'$ and the stress-like hardening variable by p_{1e} , as depicted in the upper part of Fig. 1. However, this expression is not strictly necessary for the development of the subloading models. All that matters is its evolution law.

For the normal yield function, as for the conventional Cam clay models, the internal strain-like hardening variable is given by the volumetric plastic strain ε_v^p . This relates to the “size” of the normal yield surface, given by p_{1e} , according to the following expression:

$$\dot{p}_{1e} = \frac{p_{1e}}{\chi} \dot{\varepsilon}_v^p \quad \left(\chi = \frac{\lambda - \kappa}{1 + e_0} \right) \quad (16)$$

where λ and κ are model parameters related to the virgin compression and swelling indices, respectively and e_0 is the initial void ratio.

Eq. (16) for the evolution of the normal yield surface is the same as that for the conventional Cam clay models. In Sub-Cam model, however, a new (subloading) surface is introduced and new hardening variables and hardening laws must be specified for this surface. The stress-like hardening variable, as defined previously, is the tip of the subloading surface $z_\alpha = p_1$. The corresponding strain-like hardening variable is obtained by linking the evolution of the subloading surface to that of the normal surface with an auxiliary variable ρ in the same way as proposed by Nakai & Hinokio (2004) for the Subloading tij model (to be explained in the next sub-item). This is illustrated in the lower part of Fig. 1. The variable ρ gives a measure of over-consolidation or density of a point which was previously loaded then unloaded.

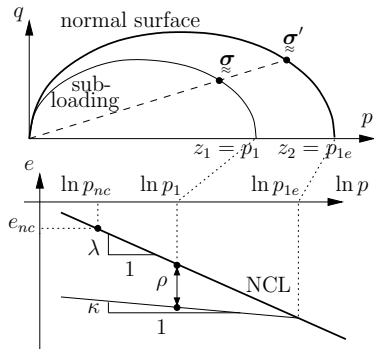


Fig.1. Subloading Cam-clay

From Fig. 1 it is possible to define the following auxiliary strain-like variable ε_v^{sy} (sy for sub-yielding) that links the subloading surface to the normal surface:

$$\varepsilon_v^{sy} = \frac{-\rho}{1 + e_0} \quad \left(\rho = (\lambda - \kappa) \ln \frac{p_{1e}}{p_1} \right) \quad (17)$$

The hardening law for the subloading surface is now given by:

$$\dot{p}_1 = \frac{p_1}{\chi} (\dot{\varepsilon}_v^p + \dot{\varepsilon}_v^{sy}) \quad \left(\chi = \frac{\lambda - \kappa}{1 + e_0} \right) \quad (18)$$

A decay function must rule the evolution of ε_v^{sy} so that the subloading surface should approach the normal surface as the point becomes less over consolidated upon reloading. Here a law similar to that proposed by Nakai & Hinokio (2004) for the subloading tij model is assumed:

$$\dot{\varepsilon}_v^{sy} = \dot{\Lambda} \frac{G(\varepsilon_v^{sy})}{p} \quad (G = c(1 + e_0)^2 (\varepsilon_v^{sy})^2) \quad (19)$$

in which c is the only additional parameter with respect to those used in the conventional Cam clay model.

Finally, the evolution laws for the internal variables of Sub-Cam model can be summarised as:

$$\begin{cases} \dot{z}_\alpha = \dot{z}_1 = \dot{p}_1 = \dot{\Lambda} \frac{p_1}{\chi} \left(\text{tr } r + \frac{G}{p} \right) = \dot{\Lambda} \mathcal{H}_1 \\ \dot{z}_\beta = \dot{z}_2 = \dot{p}_{1e} = \dot{\Lambda} \frac{p_{1e}}{\chi} \text{tr } r = \dot{\Lambda} \mathcal{H}_2 \end{cases} \quad (20)$$

All variables necessary for the computation of the elastoplastic tensor for the stress-strain evolution in Eq. (10) are also defined. The main purpose of the above formulation was to introduce the concept of subloading into the well established framework of Cam clay model. The main advantages of introducing subloading concept into Cam clay model is inclusion of the influence of density and confining pressure on the soil behaviour as well as an enhanced capacity to simulated cyclic loading at the cost of a single additional parameter. However, other drawbacks inherent to Cam clay formulation still remain and can be better overcome using the tij concept as briefly explained in the next sub-item.

2.2 Simplified Subloading tij

A series of tij models has been developed by Nakai and co-workers in Nagoya Institute of Technology (Nakai & Matsuoka, 1986; Nakai, 1989; Nakai & Hinokio, 2004). Common to all these models is the use of a modified stress quantity, named tensor tij or \underline{t} , proposed by Nakai & Mihara (1984), which is defined as:

$$\underline{t} = \underline{a} \bullet \underline{\sigma} \quad \left(\underline{a} = \sqrt{\frac{I_{3\sigma}}{I_{2\sigma}}} \underline{\tau}^{-1}; \quad \underline{\tau} = \sqrt{\underline{\sigma}} \right) \quad (21)$$

in which \underline{a} is a second order tensor related to the SMP (Spatially Mobilized Plane) introduced by Matsuoka & Nakai (1974). The SMP represents the plane in which the shear strength of the material is most mobilised on the average. Therefore, instead of using the stress invariants in the octahedral plane (p and q of Cam clay model), the models use the stress invariants on the SMP, which are denoted by the normal component t_N and the deviatoric component t_S . Using these invariants, the influence of the intermediate stresses on the strength and deformability characteristics of soils can be taken into account.

The last model of this series is the so-called Subloading tij model and a full description of the model can be found in details in Nakai & Hinokio (2004). The model also uses two yield surfaces according to the concept of subloading proposed by Hashiguchi (1989). The subloading yield surface of the model, in terms of the modified stress invariants (t_N and t_S), is given by

$$f(\underline{\sigma}, z_\alpha) = \ln \frac{t_N}{z_\alpha} + \frac{1}{\beta} \left(\frac{t_S}{M^* t_N} \right)^\beta \quad (22)$$

in which M^* is related to the parameter ϕ_{CS} (similar to M in Cam clay model) and β is an additional model parameter, which defines a unified response for the stress ratio-dilatancy relation and controls the shape of the yield function. These parameters can be obtained according to:

$$M^* = \left(X_{CS}^\beta + Y_{CS} X_{CS}^{\beta-1} \right)^{1/\beta} \quad (23)$$

in which

$$X_{CS} = \frac{\sqrt{2}}{3} \left(\sqrt{R_{CS}} - \frac{1}{\sqrt{R_{CS}}} \right); \quad Y_{CS} = \frac{1 - \sqrt{R_{CS}}}{\sqrt{2} (\sqrt{R_{CS}} + 0.5)} \quad (24)$$

and

$$R_{CS} = \left(\frac{\sigma_1}{\sigma_3} \right)_{CS(\text{compression})} = \frac{1 + \sin \phi_{CS}}{1 - \sin \phi_{CS}} \quad (25)$$

The size of the subloading surface is measured at its tip in the t_N axis as represented by $z_\alpha = t_{N1}$ in the upper part of Fig. 2.

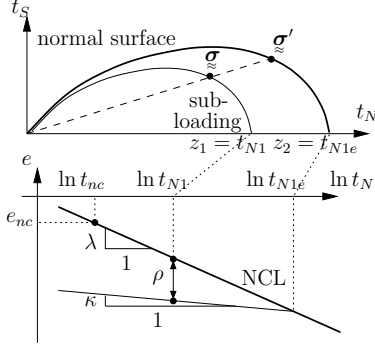


Fig.2. Subloading tij

Another common feature in tij models is the split of the plastic strain increments into two components: one given by an ‘‘associated’’ flow-rule (AF) and another due isotropic compression (IC) related to an increase of mean stress t_N . The feature is supposed to take into account the influence of stress path on the deformability characteristics of soils. However, for the sake of simplicity, this split is disregarded in this paper and only the ‘‘associated’’ flow-rule (AF) component is considered. The simplified model will be called Sub-tij, for short.

The direction of the ‘‘associated’’ flow-rule component is given by the normal to the yield surface in the modified stress space $\underline{\underline{t}}$:

$$\underline{\underline{r}} = \frac{df}{d\underline{\underline{t}}} \quad (26)$$

In fact, Eq. (26) leads to a *non-associated* flow rule in the conventional stress space $\underline{\underline{\sigma}}$. However no additional plastic potential function or parameters have to be defined for this flow rule.

The internal variables and evolution laws for Sub-tij model are defined in the same way as those for the Sub-Cam model described previously. In fact, it is just the opposite, i.e., Sub-Cam model used all hardening definitions proposed by Nakai & Hinokio (2004) for the Subloading tij model as shown in Fig. 2 and just replaced the modified mean stress invariant t_N by the conventional mean stress p :

$$\begin{cases} \dot{z}_\alpha = \dot{z}_1 = \dot{t}_{N1} = \dot{\lambda} \frac{t_{N1}}{\chi} \left(\text{tr } r + \frac{G}{t_N} \right) = \dot{\lambda} \mathcal{H}_1 \\ \dot{z}_\beta = \dot{z}_2 = \dot{t}_{N1e} = \dot{\lambda} \frac{t_{N1e}}{\chi} \text{tr } r = \dot{\lambda} \mathcal{H}_2 \end{cases} \quad (27)$$

3 INTEGRATION ALGORITHMS

The evolution laws for stress-strain and internal variables form a Differential Algebraic System which may be generically written as:

$$\begin{cases} \dot{\underline{\underline{\sigma}}} = \underline{\underline{D}}^{ep} : \dot{\underline{\underline{\varepsilon}}} \\ \dot{z}_i = \mathcal{H}_i \underline{\underline{b}} : \dot{\underline{\underline{\varepsilon}}} \end{cases} \quad (28)$$

The system is valid for rate relation or infinitesimal increments. However, in the context of real applications,

such as boundary value problems solved by the Finite Element Method, finite time steps, ΔT , and consequently finite strain increments $\Delta \underline{\underline{\varepsilon}}$, are imposed. Therefore, for a given strain increment, all the equations in the system should be integrated simultaneously. This integration can only be performed numerically using different integration schemes. Supposing that the strain rate is constant, the main objective of these schemes is to find a solution for the finite increments of stress and stress-like internal variables for a given finite strain increment as shown in the following equation:

$$\begin{cases} \Delta \underline{\underline{\sigma}} = \int_{t_n}^{t_{n+1}} \underline{\underline{D}}^{ep} : \frac{\Delta \underline{\underline{\varepsilon}}}{\Delta t} dt = \int_0^1 \underline{\underline{D}}^{ep} : \Delta \underline{\underline{\varepsilon}} dT \\ \Delta z_i = \int_{t_n}^{t_{n+1}} \mathcal{H}_i \underline{\underline{b}} : \frac{\Delta \underline{\underline{\varepsilon}}}{\Delta t} dt = \int_0^1 \mathcal{H}_i \underline{\underline{b}} : \Delta \underline{\underline{\varepsilon}} dT \end{cases} \quad (29)$$

Symbolically, Eq. (29) can be written as:

$$\{\Delta \underline{\underline{\Sigma}}\} = \left\{ \begin{matrix} \Delta \underline{\underline{\sigma}} \\ \Delta z_i \end{matrix} \right\} = \int_0^1 \{K\}(\underline{\underline{\sigma}}, z_i) dT \quad (30)$$

in which

$$\{\underline{\underline{\Sigma}}\} = \left\{ \begin{matrix} \underline{\underline{\sigma}} \\ z_i \end{matrix} \right\} \quad \text{and} \quad \{K\}(\underline{\underline{\sigma}}, z_i) = \left\{ \begin{matrix} \underline{\underline{D}}^{ep} : \Delta \underline{\underline{\varepsilon}} \\ \mathcal{H}_i \underline{\underline{b}} : \Delta \underline{\underline{\varepsilon}} \end{matrix} \right\} \quad (31)$$

The solution in Eq. (30) can be obtained using either implicit or explicit integration schemes. Here, two schemes are investigated: the Modified Euler (ME) with variable time steps and the fully implicit Backward Euler (BE).

3.1 Modified-Euler (ME) with variable time steps

Sloan (1987) presented an algorithm which automatically divides the given finite strain increment into smaller sub-increments to keep the solution within a prescribed accuracy while, at the same time, saving computational time. The algorithm was later refined and enhanced by Sloan & Booker (1992) and Sloan et al. (2001).

The key point in the Modified Euler (ME) scheme consists of computing the elastoplastic tensor and plastic moduli in two different points in the time-stress space. Here the term *stress* should be regarded in the broader sense, including the stress point and stress-like internal variables as in Eq. (31). The first point corresponds to the present stress state $(\underline{\underline{\Sigma}}_n, T_n)$. Thus a first evaluation of the stress increment, $\{\Delta \underline{\underline{\Sigma}}\}_1$ is computed. The second evaluation position is defined by $(\underline{\underline{\Sigma}}_1, T_1)$ given by a simple Forward Euler (FE), i.e., $\underline{\underline{\Sigma}}_1 = \underline{\underline{\Sigma}}_n + \{\Delta \underline{\underline{\Sigma}}\}_1$ and $T_1 = T_n + \Delta T$ as illustrated in Fig. 3. However, the stresses are not really updated, and this second point is used only to compute a second set of elastoplastic tensor and plastic moduli, from which a second estimate of stress increments, $\{\Delta \underline{\underline{\Sigma}}\}_2$, is computed

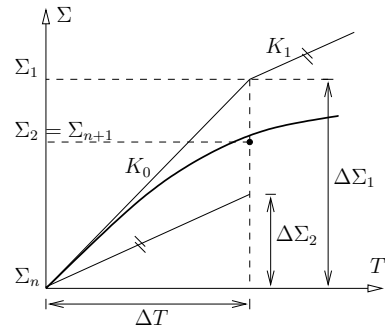


Fig.3. Modified-Euler

These derivatives may be quite cumbersome and are presented in Appendix B for the Sub-Cam and Sub-tij models defined in this paper. After a few operations, the expansion ultimately is written in matrix form as the system of equations below; see (Jeremić & Sture, 1997) and (Belytschko et al., 2000):

$$\left[A^{(k)} \right] \left\{ \Delta \Sigma^{(k)} \right\} = - \left\{ R^{(k)} \right\} - \delta \Delta \Lambda^{(k)} \left\{ r^{(k)} \right\} \quad (39)$$

where

$$\left[A^{(k)} \right] = \begin{bmatrix} (\underline{C}^e + \Delta \Lambda^{(k)} \underline{M}) & \Delta \Lambda^{(k)} \sum_{\alpha} \underline{N} & \underline{0} \\ \Delta \Lambda^{(k)} \underline{R}_{\alpha} & (\Delta \Lambda^{(k)} \sum_{\alpha} S_{\alpha\alpha} - 1) & \sum_{\beta} S_{\alpha\beta} \\ \Delta \Lambda^{(k)} \underline{R}_{\beta} & \sum_{\alpha} S_{\beta\alpha} & (\Delta \Lambda^{(k)} \sum_{\beta} S_{\beta\beta} - 1) \end{bmatrix} \quad (40)$$

and the following vectors are defined:

$$\left\{ \Delta \Sigma^{(k)} \right\} = \begin{Bmatrix} \Delta \underline{\sigma}^{(k)} \\ \Delta z_{\alpha}^{(k)} \\ \Delta z_{\beta}^{(k)} \end{Bmatrix} \quad (41)$$

$$\left\{ R^{(k)} \right\} = \begin{Bmatrix} \underline{C}^e : \underline{R}\sigma^{(k)} \\ -Rz_{\alpha}^{(k)} \\ -Rz_{\beta}^{(k)} \end{Bmatrix} \quad (42)$$

$$\left\{ r^{(k)} \right\} = \begin{Bmatrix} \underline{r}^{(k)} \\ \mathcal{H}_{\alpha}^{(k)} \\ \mathcal{H}_{\beta}^{(k)} \end{Bmatrix} \quad (43)$$

A key step in the BE algorithm is the computation of the quantity $\delta \Delta \Lambda^{(k)}$, which is obtained from the consistency condition:

$$\underline{v} : \Delta \underline{\sigma}^{(k)} + \sum_{\alpha} y_{\alpha}^{(k)} \Delta z_{\alpha}^{(k)} = -f^{(k)} \quad (44)$$

or, symbolically

$$\left\{ V^{(k)} \right\}^T \left\{ \Delta \Sigma^{(k)} \right\} = -f^{(k)} \quad (45)$$

where

$$\left\{ V^{(k)} \right\} = \begin{Bmatrix} \underline{v}^{(k)} \\ y_{\alpha}^{(k)} \\ 0 \end{Bmatrix} \quad \text{and} \quad \left\{ \Delta \Sigma^{(k)} \right\} = \begin{Bmatrix} \Delta \underline{\sigma}^{(k)} \\ \Delta z_{\alpha}^{(k)} \\ \Delta z_{\beta}^{(k)} \end{Bmatrix} \quad (46)$$

Thus, considering Eq. (39), the following expression is obtained:

$$\delta \Delta \Lambda^{(k)} = \frac{f^{(k)} - \left\{ V^{(k)} \right\}^T \left[A^{(k)} \right]^{-1} \left\{ R^{(k)} \right\}}{\left\{ V^{(k)} \right\}^T \left[A^{(k)} \right]^{-1} \left\{ r^{(k)} \right\}} \quad (47)$$

Algorithm 2 below resumes the iterative procedure for the fully implicit Backward Euler scheme. An initial solution is adopted, supposing zero increment plastic strain and yield surface sizes. That should produce errors in the residual equations, which are used to compute the estimates. The procedure continues until the solution is within a prescribed tolerance TOL_{Σ} for the error defined by:

$$Err = \frac{\left\| \begin{Bmatrix} {}^{n+1} \underline{R}\sigma^{(k)} \\ {}^{n+1} Rz_i^{(k)} \end{Bmatrix} \right\|}{\left\| n \begin{Bmatrix} \underline{\sigma} \\ z_i \end{Bmatrix} \right\|} \quad (48)$$

Algorithm 2: Fully Implicit Backward-Euler scheme

Set: TOL_{Σ}

$k \leftarrow 0$;

$\Delta \Lambda^{(0)} \leftarrow 0$;

$\underline{\sigma}^{(0)} \leftarrow n \underline{\sigma} + n \underline{D}^e : \Delta \underline{\epsilon}$;

$z_i^{(0)} \leftarrow n z_i$;

$n \{ \Sigma \} \leftarrow \left\{ \begin{matrix} \underline{\sigma} \\ z_i \end{matrix} \right\}$;

CalculateSubYieldFunction($f^{(k)}$);

repeat

 CalculateGradients($\underline{r}, \underline{v}, y_{\alpha}$);

 CalculateHighGradients($\underline{M}, \underline{N}_{\alpha}, \underline{R}_i, S_{ij}$);

 Calculate($\left[A^{(k)} \right]^{(-1)}$) Eq.(40) ;

 Calculate($\delta \Delta \Lambda$) Eq.(47) ;

 Calculate($\{ \Delta \Sigma \} = \left\{ \begin{matrix} \Delta \underline{\sigma} \\ \Delta z_i \end{matrix} \right\}$) Eq.(39) ;

$\Delta \Lambda^{(k+1)} \leftarrow \Delta \Lambda^{(k)} + \delta \Delta \Lambda$;

$\underline{\sigma}^{(k+1)} \leftarrow \underline{\sigma}^{(k)} + \Delta \underline{\sigma}$;

$z_i^{(k+1)} \leftarrow z_i^{(k)} + \Delta z_i$;

 CalculateSubYieldFunction($f^{(k+1)}$);

 CalculateResiduals(${}^{n+1} \underline{R}\sigma^{(k)}, {}^{n+1} Rz_i^{(k)}$) Eq.(37);

$Err \leftarrow \left\| \left\{ \begin{matrix} {}^{n+1} \underline{R}\sigma^{(k)} \\ {}^{n+1} Rz_i^{(k)} \end{matrix} \right\} \right\| \div \| n \{ \Sigma \} \|$;

until $Err < TOL_{\Sigma}$;

4 COMPARISON BETWEEN ME AND BE

The objective of this section is to establish which scheme, between ME and BE, can produce the most accurate solutions at the lowest computational price. The solutions given by both schemes are compared to the ‘‘exact’’ solution, which is defined as the values computed with the Forward-Euler (FE) scheme with a very large number of sub-steps (100.000). The simulations compute the final values of the stress tensor and stress-like internal variables ($\{ \Sigma \} (i) = \{ \underline{\sigma} (i) \quad z_i (i) \}^T$), for each point (i) in a grid of strain increments.

Normalised integration errors are defined for each grid point of strain increments. These errors are compared to the exact solution ($\{ \Sigma \}_c (i) = \{ \underline{\sigma}_c (i) \quad z_{ci} (i) \}^T$), according to the following expression:

$$Error_{\Sigma} (i) = \frac{\| \Sigma (i) - \Sigma_c (i) \|}{\| \Sigma_c \|} \quad (49)$$

Simulations were carried out for both Sub-Cam and Sub-tij models, assuming the parameters of Fujinomori clay (Chowdhury, 1998), which are presented in Tab. 1. In both cases the original OCR is equal to 2, i.e., the initial size of the normal yield surface was twice the size of the initial subloading surface. The value of c for the Sub-Cam model is given by c_{subcam} and for the Sub-tij model, by c_{subtij} .

Tab.1. Parameters - Fujinomori-Clay

λ	0.0891
κ	0.0196
ν	0.2
ϕ_{CS}	33.7°
e_{NC}	0.83
β	1.5
c_{subcam}	500.0
c_{subtij}	1000.0

Different initial stress positions and a large combination of strain increments were imposed to test the integration schemes. Three initial stress states over the initial (subloading) surface were specified as depicted in Fig. 5 and 6 for the models Sub-Cam and Sub-tij, respectively. Three-dimensional principal strain increments were imposed as $\Delta\varepsilon_1; \Delta\varepsilon_2; -0.5\Delta\varepsilon_3$ in a way that the corresponding final stress states increases in both deviatoric and volumetric states, i.e, moving away from the yield surface. The values of these increments are selected to create a grid of points (Fig. 7). This grid is used to plot curves of equal errors (iso-errors) with $\Delta\varepsilon_1$ in the abscissas and $\Delta\varepsilon_2$ in the ordinates.

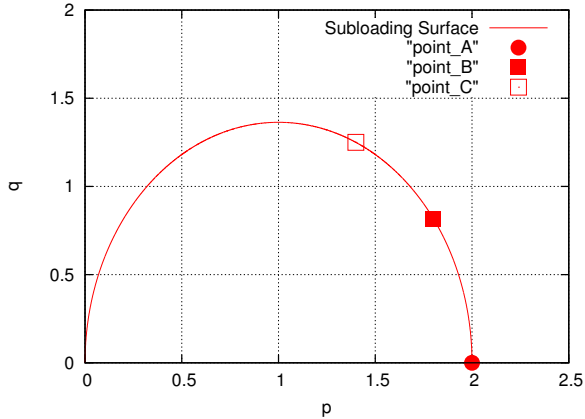


Fig.5. Subloading Cam-clay; starting points

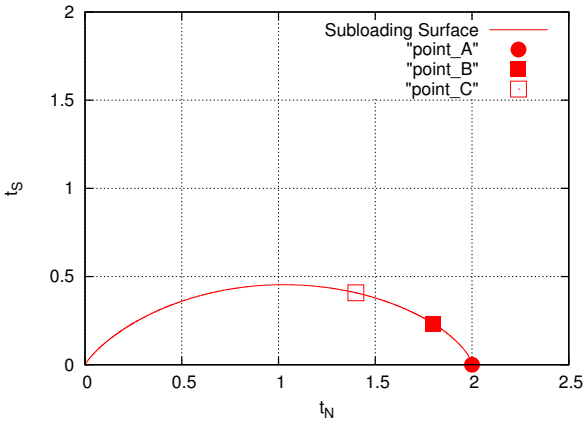


Fig.6. Subloading tij; starting points

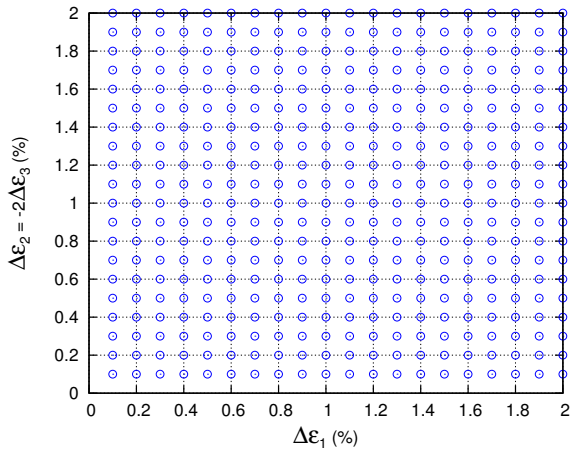


Fig.7. Mesh of imposed strain increments

For the Modified-Euler (ME) scheme, five values of tolerance $STOL$ (10^{-1} , 10^{-2} , 10^{-3} , 10^{-4} and 10^{-5}) were investigated. For the Backward-Euler (BE) scheme the values of the tolerance TOL_{Σ} were 10^{-1} , 10^{-3} , 10^{-5} , 10^{-7} and 10^{-9} and the final integration error was not much affected by this tolerance.

For each scheme and constitutive model, tables were elaborated with the summary of integration results in terms of accuracy and computational time. In these tables NSS represent the Number of Sub-Steps, computed automatically with the ME scheme; ERR represent the stress error, computed according to Eq. (49); $Time$ represent the total computational time to cover whole mesh of applied strain increments; $NDIV$ represent the number of divisions imposed to the strain increments in the BE, in order to guarantee the convergence of this scheme and to improve its accuracy; and NIT represents the number of iterations that the BE scheme took to converge, determined by trial and error.

4.1 Results for Subloading Cam clay

The results for subloading Cam clay model using the ME and BE schemes are summarised in Tab. 2 and 3, respectively. The results for both schemes show that the position of the initial stress point (A, B or C) did not influence much the accuracy and computational time of the final solution. The results also show the efficiency of the Modified Euler scheme when compared to the Backward Euler scheme.

For the range of combinations investigated the average error in the ME scheme varied from the order of 1% to 0.0001% with computational time between 0.06 seconds for the looser tolerances ($STOL = 10^{-1}$) up to 1.61 seconds for the tighter tolerances ($STOL = 10^{-5}$). On the other hand, the average errors using the BE scheme started from 4% consuming an overall time in the order of 0.18 seconds using a smaller number of sub-steps ($NDIV = 2$), while the most accurate solutions with an average error of 0.07% required $NDIV = 100$ sub-steps and demanded an overall time in the order of 6 seconds. The BE method does not allow for the automatic computation of the number of divisions necessary to guarantee its convergence.

It is worth to note that the overall average error with the ME scheme is related the local truncation error ($STOL$). In all examples run so far the overall error was at most one order of magnitude higher than $STOL$. On the other hand, the overall error with the BE scheme does not improved significantly if a tighter tolerance is set for its convergence check TOL_{Σ} and that only demands longer processing time. The accuracy of BE can only be improved by imposing smaller strain increments, but the scheme does not give any hint as to how to sub-divide the total imposed strain increment.

For the same overall average error, say ERR_{ave} in the order 0.1%, the ME scheme demanded around 0.09 seconds and the number of sub-steps was automatically computed between 5 and 12. In order to attain the same accuracy, the BE scheme requires the total strain increment to be divided in at least 100 sub-steps, taking between 2 and 3 iterations to converge and demanding around 6 seconds. This is highly inefficient considering the overall number of stress computations demanded by each scheme. The number of stress computation was at most 24 (12 steps x 2 evaluations) for the ME scheme against 300 (100 steps x 3 iterations) for the BE scheme. Thus the number of computations was at most 12.5 (300/24) times higher for the BE scheme, while the overall computational time was 66.7 (6/0.09) higher for the BE scheme. This is because the BE scheme requires the evaluation of higher order derivatives and the inversion of matrix A in Eq. (40). These operations are far more time consuming than evaluating the elastoplastic tensor and plastic moduli twice in the ME scheme.

Tab.2. Subloading Cam clay - Modified-Euler

Point	STOL	NSS_{min}	NSS_{max}	NSS_{ave}	ERR_{min} (%)	ERR_{max} (%)	ERR_{ave} (%)	Time (s)
A	1.0e-01	4	7	6	$6.36e-02$	$1.68e+00$	$1.17e+00$	0.06
A	1.0e-02	5	12	9	$5.00e-02$	$1.75e-01$	$1.24e-01$	0.09
A	1.0e-03	7	28	21	$4.92e-03$	$1.99e-02$	$1.46e-02$	0.20
A	1.0e-04	14	81	60	$6.07e-04$	$2.26e-03$	$1.57e-03$	0.54
A	1.0e-05	37	248	183	$6.59e-05$	$3.04e-04$	$1.84e-04$	1.61
B	1.0e-01	4	7	5	$4.17e-02$	$2.20e+00$	$1.27e+00$	0.05
B	1.0e-02	4	12	8	$4.17e-02$	$1.75e-01$	$1.18e-01$	0.08
B	1.0e-03	6	29	19	$4.48e-03$	$2.01e-02$	$1.35e-02$	0.18
B	1.0e-04	12	82	53	$5.87e-04$	$2.23e-03$	$1.44e-03$	0.47
B	1.0e-05	31	249	160	$5.05e-05$	$3.23e-04$	$1.63e-04$	1.40
C	1.0e-01	4	7	5	$2.79e-02$	$2.41e+00$	$1.44e+00$	0.05
C	1.0e-02	4	12	9	$2.79e-02$	$1.83e-01$	$1.34e-01$	0.08
C	1.0e-03	6	29	20	$4.85e-03$	$2.05e-02$	$1.54e-02$	0.18
C	1.0e-04	11	82	55	$5.79e-04$	$2.27e-03$	$1.65e-03$	0.49
C	1.0e-05	28	251	170	$6.33e-05$	$3.43e-04$	$1.98e-04$	1.49

Tab.3. Subloading Cam clay - Backward-Euler - $TOL_{\Sigma} = 10^{-3}, 10^{-5}, 10^{-7}$

Point	NDIV	TOL_{Σ}	NIT_{min}	NIT_{max}	NIT_{ave}	ERR_{min} (%)	ERR_{max} (%)	ERR_{ave} (%)	Time (s)
A	2	1.0e-03	2	8	4	$2.39e-01$	$1.15e+01$	$3.87e+00$	0.18
A	5	1.0e-03	1	4	2	$1.08e-01$	$3.77e+00$	$1.47e+00$	0.31
A	10	1.0e-03	1	3	2	$7.95e-02$	$1.80e+00$	$7.19e-01$	0.55
A	100	1.0e-03	1	2	1	$8.21e-03$	$1.30e+00$	$5.47e-01$	2.65
A	2	1.0e-05	3	18	7	$2.45e-01$	$1.14e+01$	$3.87e+00$	0.28
A	5	1.0e-05	2	6	4	$1.03e-01$	$3.78e+00$	$1.44e+00$	0.44
A	10	1.0e-05	2	4	3	$5.27e-02$	$1.79e+00$	$7.03e-01$	0.67
A	100	1.0e-05	1	2	1	$8.21e-03$	$1.99e-01$	$7.55e-02$	4.43
A	2	1.0e-07	4	28	10	$2.45e-01$	$1.14e+01$	$3.87e+00$	0.40
A	5	1.0e-07	3	8	5	$1.04e-01$	$3.78e+00$	$1.44e+00$	0.57
A	10	1.0e-07	3	6	4	$5.29e-02$	$1.79e+00$	$7.04e-01$	0.95
A	100	1.0e-07	2	3	2	$5.39e-03$	$1.71e-01$	$6.92e-02$	6.08
B	2	1.0e-03	2	8	4	$1.79e-01$	$1.13e+01$	$3.68e+00$	0.18
B	5	1.0e-03	1	4	2	$9.42e-02$	$3.76e+00$	$1.39e+00$	0.31
B	10	1.0e-03	1	3	2	$7.10e-02$	$1.79e+00$	$6.87e-01$	0.54
B	100	1.0e-03	1	2	1	$7.39e-03$	$1.32e+00$	$5.39e-01$	2.64
B	2	1.0e-05	3	19	6	$1.83e-01$	$1.14e+01$	$3.68e+00$	0.28
B	5	1.0e-05	2	6	4	$7.64e-02$	$3.78e+00$	$1.35e+00$	0.43
B	10	1.0e-05	2	4	3	$3.90e-02$	$1.78e+00$	$6.58e-01$	0.66
B	100	1.0e-05	1	2	1	$7.31e-03$	$1.99e-01$	$7.11e-02$	4.42
B	2	1.0e-07	4	30	10	$1.83e-01$	$1.14e+01$	$3.68e+00$	0.40
B	5	1.0e-07	3	8	5	$7.69e-02$	$3.78e+00$	$1.35e+00$	0.57
B	10	1.0e-07	3	5	4	$3.91e-02$	$1.78e+00$	$6.59e-01$	0.95
B	100	1.0e-07	2	3	2	$3.98e-03$	$1.70e-01$	$6.45e-02$	6.09
C	2	1.0e-03	2	9	4	$9.75e-02$	$1.23e+01$	$3.99e+00$	0.18
C	5	1.0e-03	1	4	2	$9.68e-02$	$4.15e+00$	$1.54e+00$	0.31
C	10	1.0e-03	1	3	2	$7.04e-02$	$1.99e+00$	$7.81e-01$	0.53
C	100	1.0e-03	1	2	1	$7.24e-03$	$1.24e+00$	$5.15e-01$	2.63
C	2	1.0e-05	3	20	7	$9.33e-02$	$1.22e+01$	$3.98e+00$	0.29
C	5	1.0e-05	2	6	4	$3.93e-02$	$4.13e+00$	$1.51e+00$	0.42
C	10	1.0e-05	2	4	3	$1.96e-02$	$1.98e+00$	$7.42e-01$	0.66
C	100	1.0e-05	1	2	1	$7.24e-03$	$2.17e-01$	$7.96e-02$	4.40
C	2	1.0e-07	4	31	10	$9.32e-02$	$1.22e+01$	$3.98e+00$	0.40
C	5	1.0e-07	3	8	5	$3.83e-02$	$4.14e+00$	$1.51e+00$	0.58
C	10	1.0e-07	3	5	4	$1.93e-02$	$1.98e+00$	$7.43e-01$	0.94
C	100	1.0e-07	2	3	2	$1.95e-03$	$1.90e-01$	$7.35e-02$	6.04

The difference between the accuracy of the two methods can be better visualised using the iso-error contours shown in Figs. 8 to 11 for some specific cases of $STOL$ and $NDIV$. In these figures, it is possible to note that the magnitude of errors is much higher in the Backward-Euler scheme. Also the overall average error increases with the norm of the imposed strain increments especially for the BE scheme, while it is better distributed for the ME scheme.

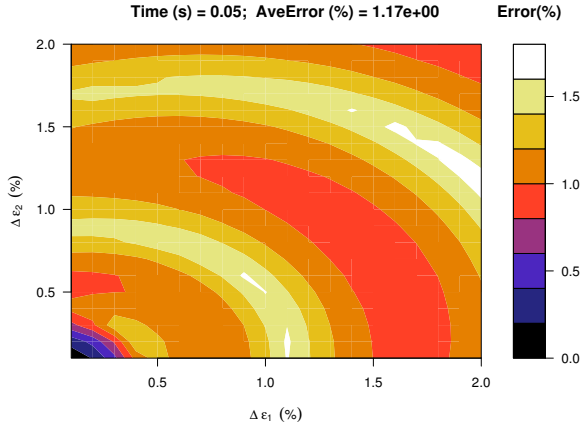


Fig.8. Subloading Cam-clay; point A; Modified-Euler; $STOL = 10^{-1}$

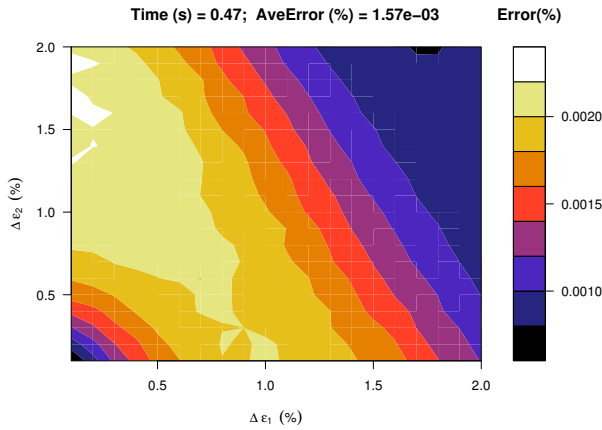


Fig.9. Subloading Cam-clay; point A; Modified-Euler; $STOL = 10^{-4}$

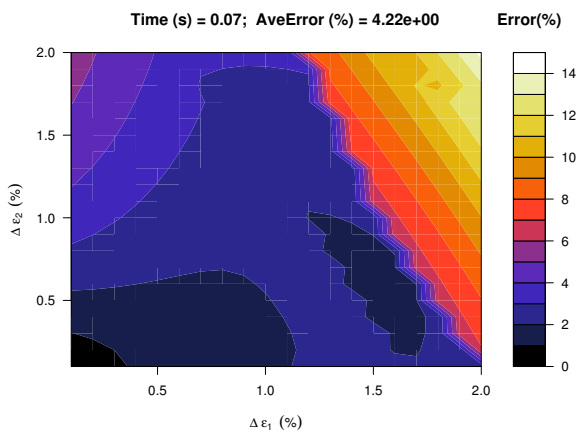


Fig.10. Subloading Cam-clay; point A; Backward-Euler; $NDIV = 2; TOL_{\Sigma} = 10^{-1}$

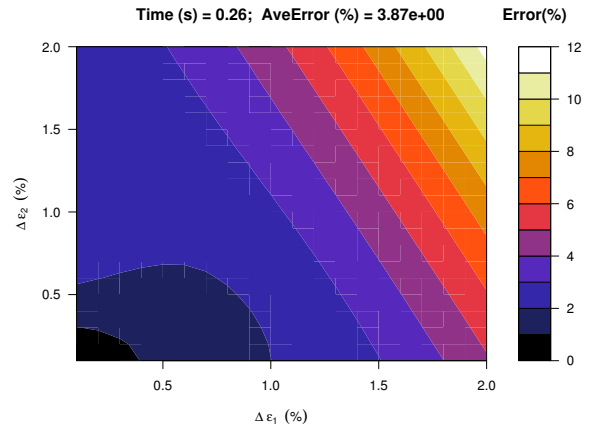


Fig.11. Subloading Cam-clay; point A; Backward-Euler; $NDIV = 2; TOL_{\Sigma} = 10^{-5}$

4.2 Results for Subloading tij

The results for the model Sub-tij, integrated with Modified-Euler (ME) and Backward-Euler (BE), are summarised in Tabs. 4 and 5, respectively. In both cases the order of error and computational time did not change much for the initial stress points at A, B or C. Comparing the two tables overall, it can be observed again that the ME scheme with automatic step size is far more accurate and efficient than the BE scheme. Errors for the ME scheme varied in the range from 1% to $10^{-4}\%$, while for the BE scheme the average errors varied between 4% and $10^{-2}\%$. Besides, the BE scheme took far longer to integrate the whole mesh of imposed strains; while the computational time varied between 0.19 and 5.05 seconds for the ME scheme, the BE scheme took between 8.79 and 245 seconds.

The error distribution can be better appreciated with the iso-error curves shown in Figs. 12 to 15, for the initial stress point at A, B or C and different values of $STOL$ for the ME scheme and $NDIV$ for the BE scheme. Again it can be noted that the magnitude of the error with the Backward Euler scheme was far higher than those for the ME scheme, reaching in some cases maximum errors in the order of 20%. Also the errors for the BE scheme increase with the norm of the imposed strain increments, while being better distributed for the ME scheme.

It is also interesting to compare the performance of both ME and BE schemes when integrating both Sub-cam and Sub-tij models. From Tabs. 2 and 4, both for the ME scheme, it is noted that the computational time is larger for integrating the subloading tij model, although keeping the same order of magnitude. However, the time difference was one order of magnitude larger for the BE scheme (tables 3 and 5). This is because the gradients are more complex in the subloading tij model and also it demands the computation of eigen-values and eigen-projectors which are not necessary in the Sub-cam model.

When comparing the iso-error figures for the two models with the same integration schemes, it can be also noted that the integration errors are higher for the subloading tij model. The difference is more noticeable for the BE scheme, but overall the subloading tij model is harder to integrate than the subloading Cam clay model. Perhaps, this is related to the tougher restrictions for the stress domain in models using tij modified stress, since the principal stresses can never become negative.

Tab.4. Subloading tij - Modified-Euler

Point	STOL	NSS_{min}	NSS_{max}	NSS_{ave}	ERR_{min} (%)	ERR_{max} (%)	ERR_{ave} (%)	Time (s)
A	1.0e-01	4	7	5	$1.84e-01$	$3.40e+00$	$1.59e+00$	0.19
A	1.0e-02	5	12	9	$4.53e-02$	$3.05e-01$	$2.03e-01$	0.30
A	1.0e-03	8	28	20	$1.17e-02$	$3.77e-02$	$2.82e-02$	0.63
A	1.0e-04	17	79	57	$1.65e-03$	$4.12e-03$	$3.23e-03$	1.69
A	1.0e-05	44	242	172	$8.81e-05$	$3.84e-04$	$2.52e-04$	5.05
B	1.0e-01	4	7	6	$2.54e-01$	$5.43e+00$	$2.81e+00$	0.20
B	1.0e-02	6	15	11	$8.91e-02$	$3.04e-01$	$2.13e-01$	0.36
B	1.0e-03	9	32	25	$1.07e-02$	$2.88e-02$	$1.78e-02$	0.78
B	1.0e-04	18	91	67	$7.85e-04$	$2.78e-03$	$1.57e-03$	2.03
B	1.0e-05	53	281	207	$1.42e-04$	$6.69e-04$	$3.15e-04$	6.17
C	1.0e-01	4	7	6	$8.17e-02$	$7.49e+00$	$5.31e+00$	0.30
C	1.0e-02	5	15	12	$7.90e-02$	$6.19e-01$	$3.27e-01$	0.38
C	1.0e-03	7	36	26	$8.24e-03$	$3.66e-02$	$2.93e-02$	0.80
C	1.0e-04	14	100	75	$9.34e-04$	$3.49e-03$	$2.52e-03$	2.22
C	1.0e-05	41	310	230	$8.29e-05$	$8.90e-04$	$3.81e-04$	6.87

Tab.5. Subloading tij - Backward-Euler - $TOL_{\Sigma} = 10^{-3}, 10^{-5}, 10^{-7}$

Point	NDIV	TOL_{Σ}	NIT_{min}	NIT_{max}	NIT_{ave}	ERR_{min} (%)	ERR_{max} (%)	ERR_{ave} (%)	Time (s)
A	2	1.0e-03	2	6	4	$3.31e-01$	$1.31e+01$	$4.44e+00$	8.79
A	5	1.0e-03	1	5	2	$2.39e-01$	$4.31e+00$	$1.67e+00$	13.87
A	10	1.0e-03	1	3	2	$1.71e-01$	$2.07e+00$	$8.29e-01$	21.29
A	100	1.0e-03	1	1	1	$1.80e-02$	$1.65e+00$	$7.05e-01$	94.27
A	2	1.0e-05	2	8	6	$3.29e-01$	$1.31e+01$	$4.43e+00$	11.55
A	5	1.0e-05	2	6	4	$1.53e-01$	$4.35e+00$	$1.66e+00$	19.65
A	10	1.0e-05	2	4	3	$8.18e-02$	$2.06e+00$	$8.16e-01$	30.83
A	100	1.0e-05	1	2	1	$1.80e-02$	$2.03e-01$	$8.30e-02$	183.75
A	2	1.0e-07	4	10	7	$3.28e-01$	$1.31e+01$	$4.43e+00$	14.45
A	5	1.0e-07	2	7	5	$1.52e-01$	$4.35e+00$	$1.66e+00$	25.07
A	10	1.0e-07	2	5	4	$8.17e-02$	$2.06e+00$	$8.15e-01$	40.25
A	100	1.0e-07	2	3	2	$8.96e-03$	$1.96e-01$	$8.09e-02$	245.62
B	2	1.0e-03	2	6	4	$2.80e-01$	$1.34e+01$	$4.55e+00$	8.76
B	5	1.0e-03	1	4	2	$1.94e-01$	$4.42e+00$	$1.73e+00$	13.62
B	10	1.0e-03	1	3	2	$9.90e-02$	$2.12e+00$	$8.53e-01$	21.23
B	100	1.0e-03	1	1	1	$1.01e-02$	$1.63e+00$	$6.95e-01$	94.90
B	2	1.0e-05	2	9	6	$2.77e-01$	$1.34e+01$	$4.54e+00$	11.69
B	5	1.0e-05	2	6	4	$1.22e-01$	$4.44e+00$	$1.71e+00$	19.53
B	10	1.0e-05	2	5	3	$6.26e-02$	$2.11e+00$	$8.50e-01$	30.74
B	100	1.0e-05	1	2	1	$1.01e-02$	$2.10e-01$	$8.60e-02$	184.59
B	2	1.0e-07	4	11	7	$2.77e-01$	$1.34e+01$	$4.54e+00$	14.53
B	5	1.0e-07	3	7	5	$1.21e-01$	$4.44e+00$	$1.71e+00$	24.99
B	10	1.0e-07	2	6	4	$6.24e-02$	$2.11e+00$	$8.50e-01$	40.41
B	100	1.0e-07	2	3	2	$6.43e-03$	$2.03e-01$	$8.43e-02$	252.30
C	2	1.0e-03	2	7	4	$1.69e-01$	$1.45e+01$	$4.90e+00$	10.26
C	5	1.0e-03	1	4	2	$1.22e-01$	$4.92e+00$	$1.97e+00$	20.01
C	10	1.0e-03	1	3	2	$6.20e-02$	$2.46e+00$	$1.00e+00$	25.16
C	100	1.0e-03	1	1	1	$6.29e-03$	$1.62e+00$	$6.77e-01$	93.74
C	2	1.0e-05	3	9	6	$1.65e-01$	$1.44e+01$	$4.88e+00$	11.44
C	5	1.0e-05	2	6	4	$7.20e-02$	$4.96e+00$	$1.96e+00$	19.75
C	10	1.0e-05	2	6	3	$3.74e-02$	$2.46e+00$	$1.00e-00$	31.73
C	100	1.0e-05	1	3	1	$6.29e-03$	$2.44e-01$	$9.93e-02$	186.76
C	2	1.0e-07	4	12	7	$1.65e-01$	$1.44e+01$	$4.88e+00$	16.70
C	5	1.0e-07	3	8	5	$7.18e-02$	$4.96e+00$	$1.96e+00$	27.92
C	10	1.0e-07	3	8	4	$3.69e-02$	$2.46e+00$	$1.00e-00$	42.30
C	100	1.0e-07	2	4	2	$3.79e-03$	$2.37e-01$	$9.82e-02$	257.52

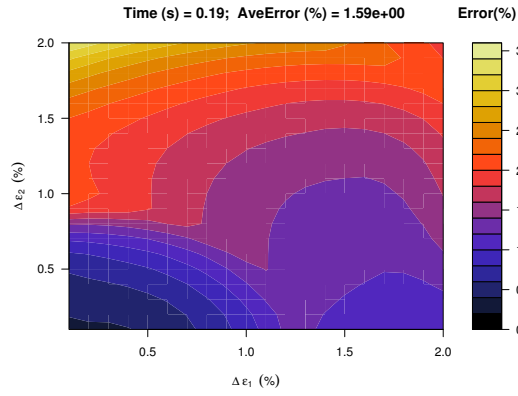


Fig.12. Subtij; point A; ME; $STOL = 1E - 1$

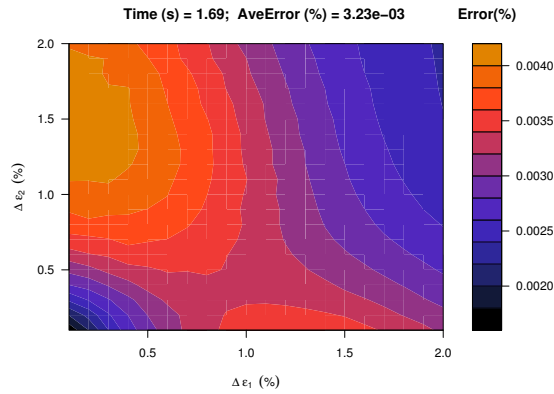


Fig.13. Subtij; point A; ME; $STOL = 1E - 4$

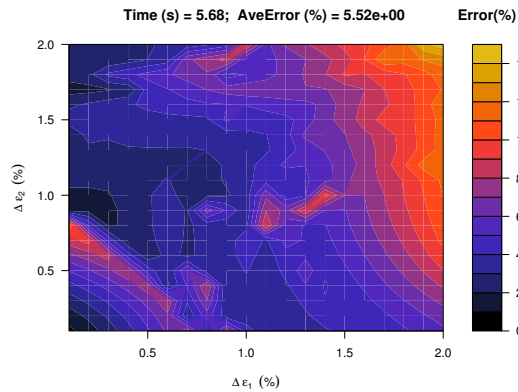


Fig.14. Subtij; point A; BE; $NDIV = 2$; $TOL_{\Sigma} = 10^{-1}$

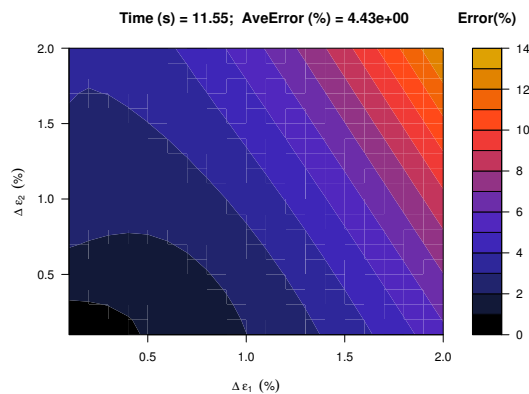


Fig.15. Subtij; point A; BE; $NDIV = 2$; $TOL_{\Sigma} = 10^{-5}$

5 CONCLUSIONS

Two numerical integration schemes, namely the explicit Modified-Euler (ME) with automatic time-step and the fully implicit Backward-Euler (BE), were applied to integrate the evolution laws of two constitutive models based in the subloading concept, namely the Subloading Cam clay model and the Subloading tij model.

Both models were formulated within the same framework, using the concept of internal hardening variables (stress-like and strain-like). Therefore the integration schemes can be applied to any elastoplastic model formulated in this way, no matter the number of yield surface used. Also it is important to emphasise that the evolution laws for the stress-strain relation and for the internal hardening variables should be integrated simultaneously in a coupled way.

The Modified Euler scheme with automatic time step proved to be extremely versatile and easy to implement. It always gave the most accurate solutions at the shortest possible computational time.

The automatic time stepping algorithm is fundamental to keep the accuracy of the solution and is controlled by a single local error tolerance ($STOL$). This rids the user of the difficult task of predefining the number of steps into which the integration algorithm should sub-divide a given strain increment. The examples run in this paper showed that the overall average error when integrating over a determined grid of imposed strain increment was within one order of magnitude higher than $STOL$. This gives an important clue as to which value to choose for $STOL$, according to the desired overall accuracy.

The fully implicit Backward Euler (BE) scheme resulted in an integrator which is overall slow, inaccurate and hard to implement. This scheme can not guarantee convergence for a given strain increment and in most cases the total increment has to be divided into a number of smaller steps. However, the BE scheme does not allow for any measure which can be used to automatically compute the number of divisions necessary for its convergence or to assure a desired accuracy level. In practice, this can only be done in a trial and error basis, leading to unnecessary computations.

The longer time demanded by the BE scheme is clearly related to the need to evaluate higher order derivatives and due to the iterative process necessary to reach convergence. In the case of Subloading tij model the computational time demanded by the BE scheme is even higher, since the derivatives in this model requires the time-consuming evaluation of eigen-values and eigen-projectors.

For the values of initial stresses and imposed mesh of strain increments investigated in this paper both ME and BE schemes were stable. The initial stress position did not affect much the overall accuracy and computational time in both schemes. However, the magnitude of the integration error increases with the norm of imposed strain increments, especially in the case of using the BE scheme.

Both schemes could be applied to Subloading Cam clay and Subloading tij models. However, the later demanded longer time and resulted in poorer accuracy, especially when integrated with the BE scheme. Overall the Subloading tij model seems harder to integrate, perhaps due to the more restrict stress range imposed by the modified stress tensor tij.

6 ACKNOWLEDGEMENTS

The authors acknowledge the financial support of the Brazilian National Research Council (CNPq). Special thanks are given to professor Teruo Nakai, of Nagoya Institute of Technology, Japan, with whom the authors keep close cooperation.

REFERENCES

- Belytschko, T., Liu, W. K., & Moran, B. (2000). *Nonlinear Finite Elements for Continua and Structures*. John Wiley and Sons, Chichester, England, 650 pp.
- Buttner, J. & Simeon, B. (2002). Runge-kutta methods in elastoplasticity. *Applied Numerical Mathematics*, 41:443–458.
- Chowdhury, E. Q. (1998). *Elastoplastic Models for Clays Under Monotonic and Cyclic Loading Using Conventional and Modified Stresses*. Master's thesis, Nagoya Institute of Technology, Nagoya, Japan.
- Desai, C. S. & Siriwardane, H. J. (1984). *Constitutive Laws for Engineering Materials With Emphasis on Geologic Materials*. Prentice-Hall, Englewood Cliffs, USA, 464 pp.
- Hashiguchi, K. (1989). Subloading surface model in unconventional plasticity. *International Journal of Solids and Structures*, 25(8):917–945.
- Hashiguchi, K. & Ueno, M. (1977). Elastoplastic constitutive laws of soils. In *Proc. 9th ICSMFE, Special Session 9*. Tokyo, pp. 73–82.
- Jeremić, B. & Sture, S. (1997). Implicit integrations in elasto-plastic geotechnics. *International Journal for Mechanics of Choesive-Frictional Materials and Structures*, 2:165–183.
- Matsuoka, H. & Nakai, T. (1974). Stress-deformation and strength characteristics of soil under three different principal stresses. In *Proc. JSCE*. p. 232.
- Miehe, C. (1997). Comparison of two algorithms for the computation of fourth-order isotropic tensor functions. *Computers and Structures*, 66(1):37–43.
- Nakai, T. (1989). An isotropic hardening elastoplastic model for sand considering the stress path dependency in three-dimensional stresses. *Soils and Foundations*, 29(1):119–137.
- Nakai, T. & Hinokio, M. (2004). A simple elastoplastic model for normally and over consolidated soils with unified material parameters. *Soil and Foundations*, 44(2):12–30.
- Nakai, T. & Matsuoka, H. (1986). A generalized elastoplastic constitutive model for clay in three-dimensional stresses. *Soil and Foundations*, 26(3):81–98.
- Nakai, T. & Mihara, Y. (1984). A new mechanical quantity for soils and its application to elastoplastic constitutive models. *Soil and Foundations*, 24(2):82–94.
- Pedroso, D. M. (2002). *Elastoplastic Models for Clayey Soils: Behavior Forecast Capacity and Constitutive Relation Integration*. Master's thesis, University of Brasilia. In portuguese.
- Simo, J. C. (1994). *Topics on the Numerical Analysis and Simulation of Plasticity*. Elsevier, USA, 315 pp.
- Simo, J. C. & Hughes, T. J. R. (1998). *Computational Inelasticity*. Springer, USA, 392 pp.
- Sloan, S. W. (1987). Substepping schemes for the numerical integration of elastoplastic stress-strain relations. *International Journal for Numerical Methods in Engineering*, 24:893–911.
- Sloan, S. W., Abbo, A. J., & Sheng, D. (2001). Refined explicit integration of elastoplastic models with automatic error control. *Engineering Computations*, 18:121–154.
- Sloan, S. W. & Booker, J. R. (1992). Integration of tresca and mohr-coulomb constitutive relations in plane strain elastoplasticity. *International Journal for Numerical Methods in Engineering*, 33:163–196.

A APPENDIX

The definitions in this paper use a system of Cartesian coordinates and an orthonormal basis. Direct or Gibbs notation is used to facilitate the understanding of the physical meaning of the equations. Although a bit cumbersome,

the piling of under tildes is used to indicate the order of an entity. The following operations are defined:

$$\begin{aligned}
 \underline{\underline{a}} &= a_i \underline{\underline{e}}_i \\
 \underline{\underline{a}} \bullet \underline{\underline{b}} &= a_i b_i = s \\
 \|\underline{\underline{a}}\|_2 &= \sqrt{\underline{\underline{a}} \bullet \underline{\underline{a}}} \\
 (\underline{\underline{a}} \otimes \underline{\underline{b}}) \bullet \underline{\underline{c}} &= \underline{\underline{a}}(\underline{\underline{b}} \bullet \underline{\underline{c}}) \\
 \underline{\underline{a}} \otimes \underline{\underline{b}} &= a_i b_j \underline{\underline{e}}_i \otimes \underline{\underline{e}}_j \\
 \underline{\underline{A}} &= A_{ij} \underline{\underline{e}}_i \otimes \underline{\underline{e}}_j \\
 \underline{\underline{A}} : \underline{\underline{B}} &= A_{ij} B_{ij} = S \\
 \|\underline{\underline{A}}\|_2 &= \sqrt{\underline{\underline{A}} : \underline{\underline{A}}} \\
 \underline{\underline{M}} &= M_{ijk} \underline{\underline{e}}_i \otimes \underline{\underline{e}}_j \otimes \underline{\underline{e}}_k \\
 \underline{\underline{a}} \otimes \underline{\underline{A}} &= a_i A_{jk} \underline{\underline{e}}_i \otimes \underline{\underline{e}}_j \otimes \underline{\underline{e}}_k \\
 \underline{\underline{A}} \otimes \underline{\underline{a}} &= A_{ij} a_k \underline{\underline{e}}_i \otimes \underline{\underline{e}}_j \otimes \underline{\underline{e}}_k \\
 \underline{\underline{T}} &= T_{ijkl} \underline{\underline{e}}_i \otimes \underline{\underline{e}}_j \otimes \underline{\underline{e}}_k \otimes \underline{\underline{e}}_l \\
 (\underline{\underline{A}} \otimes \underline{\underline{B}}) : \underline{\underline{C}} &= \underline{\underline{A}}(\underline{\underline{B}} : \underline{\underline{C}}) \\
 \underline{\underline{A}} \otimes \underline{\underline{B}} &= A_{ij} B_{kl} \underline{\underline{e}}_i \otimes \underline{\underline{e}}_j \otimes \underline{\underline{e}}_k \otimes \underline{\underline{e}}_l \\
 \underline{\underline{A}} \bullet \underline{\underline{B}} &= A_{im} B_{mj} \underline{\underline{e}}_i \otimes \underline{\underline{e}}_j \\
 \underline{\underline{A}} \bullet \underline{\underline{a}} &= A_{im} a_m \underline{\underline{e}}_i \\
 \underline{\underline{a}} \bullet \underline{\underline{T}} &= a_m T_{mijk} \underline{\underline{e}}_i \otimes \underline{\underline{e}}_j \otimes \underline{\underline{e}}_k \\
 \underline{\underline{M}} \bullet \underline{\underline{A}} &= M_{ijm} A_{mk} \underline{\underline{e}}_i \otimes \underline{\underline{e}}_j \otimes \underline{\underline{e}}_k \\
 \underline{\underline{T}} \bullet \underline{\underline{A}} &= T_{ijkm} A_{ml} \underline{\underline{e}}_i \otimes \underline{\underline{e}}_j \otimes \underline{\underline{e}}_k \otimes \underline{\underline{e}}_l \\
 \underline{\underline{A}} \otimes \underline{\underline{B}} &= A_{ik} B_{jl} \underline{\underline{e}}_i \otimes \underline{\underline{e}}_j \otimes \underline{\underline{e}}_k \otimes \underline{\underline{e}}_l \\
 \underline{\underline{A}} \boxtimes \underline{\underline{B}} &= A_{il} B_{jk} \underline{\underline{e}}_i \otimes \underline{\underline{e}}_j \otimes \underline{\underline{e}}_k \otimes \underline{\underline{e}}_l
 \end{aligned}$$

With the present notation it is easy to realize the final order of a “dot” product. The number of undertildes of each tensor is added and each dot drops two tildes of the final result. Thus, a dot (\bullet) drops two tildes and two dots ($:$) drops four tildes. In the dyadic products (x or * symbols encased in a circle or square) the final order is simply the sum of the number of tildes of the operands.

B APPENDIX

All the derivatives necessary to the definition of the evolution laws and their integration for both Subloading Cam clay and Subloading tij models are given in this appendix. For both models the following equation is used:

$$k = 2c(\lambda - \kappa)^2 \log \frac{z_\beta}{z_\alpha} \quad (50)$$

B.1 Subloading Cam-clay

$$\underline{\underline{M}} = \left(\frac{2M^2}{9} - 1 \right) \underline{\underline{I}} \otimes \underline{\underline{I}} + 3 \underline{\underline{I}}^{sym} \quad (51)$$

$$\underline{\underline{N}}_1 = \frac{-M^2}{3} \underline{\underline{I}} \quad (52)$$

$$\underline{\underline{R}}_1 = \frac{p_1}{\chi} \left(\frac{2M^2}{3} - \frac{G}{3p^2} \right) \underline{\underline{I}} \quad (53)$$

$$\underline{\underline{R}}_2 = \frac{p_{1e}}{\chi} \frac{2M^2}{3} \underline{\underline{I}} \quad (54)$$

$$S_{11} = \frac{tr(\underline{\underline{r}})}{\chi} + \frac{G - k}{p\chi} \quad (55)$$

$$S_{12} = \frac{p_1 k}{p_{1e} p \chi} \quad (56)$$

$$S_{21} = 0 \quad (57)$$

$$S_{22} = \frac{\text{tr}(\underline{\mathbf{r}})}{\chi} \quad (58)$$

B.2 Subloading t_{ij}

Some of the following equations were deduced in Pedroso (2002). The derivatives of eigen-projectors with respect to the stress tensors are based on the work of (Miehe, 1997).

$$\begin{aligned} \underline{\underline{\mathbf{M}}} &= \frac{dt_N}{d\underline{\underline{\boldsymbol{\sigma}}}} \otimes \frac{\partial^2 f}{\partial t_N \partial \underline{\underline{\boldsymbol{\sigma}}}} + \frac{\partial f}{\partial t_N} \frac{\partial^2 t_N}{\partial \underline{\underline{\boldsymbol{\sigma}}} \partial \underline{\underline{\boldsymbol{\sigma}}}} \\ &+ \frac{dt_S}{d\underline{\underline{\boldsymbol{\sigma}}}} \otimes \frac{\partial^2 f}{\partial t_S \partial \underline{\underline{\boldsymbol{\sigma}}}} + \frac{\partial f}{\partial t_S} \frac{\partial^2 t_S}{\partial \underline{\underline{\boldsymbol{\sigma}}} \partial \underline{\underline{\boldsymbol{\sigma}}}} \end{aligned} \quad (59)$$

in which

$$\frac{dt_N}{d\underline{\underline{\boldsymbol{\sigma}}}} = \underline{\underline{\mathbf{a}}} \quad (60)$$

$$\frac{dt_S}{d\underline{\underline{\boldsymbol{\sigma}}}} = \frac{\underline{\underline{t}} - t_N \underline{\underline{\mathbf{a}}}}{t_S} \quad (61)$$

$$\frac{dt_N}{d\underline{\underline{\boldsymbol{\sigma}}}} = \frac{-t_N}{I_{2\sigma}} \frac{dI_{2\sigma}}{d\underline{\underline{\boldsymbol{\sigma}}}} + \frac{3}{I_{2\sigma}} \frac{dI_{3\sigma}}{d\underline{\underline{\boldsymbol{\sigma}}}} \quad (62)$$

$$\frac{dt_S}{d\underline{\underline{\boldsymbol{\sigma}}}} = \frac{t_N}{6t_S} \frac{dI_{1\sigma}}{d\underline{\underline{\boldsymbol{\sigma}}}} + \frac{t_N(6t_N - I_{1\sigma})}{6t_S I_{2\sigma}} \frac{dI_{2\sigma}}{d\underline{\underline{\boldsymbol{\sigma}}}} + \frac{I_{1\sigma} - 6t_N}{2t_S I_{2\sigma}} \frac{dI_{3\sigma}}{d\underline{\underline{\boldsymbol{\sigma}}}} \quad (63)$$

$$\frac{\partial^2 f}{\partial t_N \partial \underline{\underline{\boldsymbol{\sigma}}}} = \frac{(\beta + 1)\phi - 1}{t_N^2} \frac{dt_N}{d\underline{\underline{\boldsymbol{\sigma}}}} + \frac{-\beta\phi}{t_N t_S} \frac{dt_S}{d\underline{\underline{\boldsymbol{\sigma}}}} \quad (64)$$

$$\frac{\partial^2 f}{\partial t_S \partial \underline{\underline{\boldsymbol{\sigma}}}} = \frac{-\beta\phi}{t_N t_S} \frac{dt_N}{d\underline{\underline{\boldsymbol{\sigma}}}} + \frac{(\beta - 1)\phi}{t_S^2} \frac{dt_S}{d\underline{\underline{\boldsymbol{\sigma}}}} \quad (65)$$

$$\frac{\partial^2 t_N}{\partial \underline{\underline{\boldsymbol{\sigma}}} \partial \underline{\underline{\boldsymbol{\sigma}}}} = \frac{d\underline{\underline{\mathbf{a}}}}{d\underline{\underline{\boldsymbol{\sigma}}}} \quad (66)$$

$$\frac{\partial^2 t_S}{\partial \underline{\underline{\boldsymbol{\sigma}}} \partial \underline{\underline{\boldsymbol{\sigma}}}} = \frac{-1}{t_S^2} \underline{\underline{t}} \otimes \frac{dt_S}{d\underline{\underline{\boldsymbol{\sigma}}}} + \frac{1}{t_S} \frac{d\underline{\underline{\mathbf{t}}}}{d\underline{\underline{\boldsymbol{\sigma}}}} \quad (67)$$

$$- \underline{\underline{\mathbf{a}}} \otimes \left(\frac{1}{t_S} \frac{dt_N}{d\underline{\underline{\boldsymbol{\sigma}}}} - \frac{t_N}{t_S^2} \frac{dt_S}{d\underline{\underline{\boldsymbol{\sigma}}}} \right) - \frac{t_N}{t_S} \frac{d\underline{\underline{\mathbf{a}}}}{d\underline{\underline{\boldsymbol{\sigma}}}}$$

$$\underline{\underline{\boldsymbol{\tau}}} = \sqrt{\underline{\underline{\boldsymbol{\sigma}}}} \quad (68)$$

$$\underline{\underline{\mathbf{a}}} = \sqrt{\frac{I_{3\sigma}}{I_{2\sigma}}} \underline{\underline{\boldsymbol{\tau}}}^{-1} = r_z \underline{\underline{\boldsymbol{\tau}}}^{-1} \quad (69)$$

$$\frac{d\underline{\underline{\mathbf{a}}}}{d\underline{\underline{\boldsymbol{\sigma}}}} = \underline{\underline{\boldsymbol{\tau}}}^{-1} \otimes \left(\frac{1}{2\sqrt{\frac{I_{3\sigma}}{I_{2\sigma}}}} \frac{dI_{3\sigma}}{d\underline{\underline{\boldsymbol{\sigma}}}} - \frac{I_{3\sigma}}{2\sqrt{\frac{I_{3\sigma}}{I_{2\sigma}}}} \frac{dI_{2\sigma}}{d\underline{\underline{\boldsymbol{\sigma}}}} \right) \quad (70)$$

$$+ \sqrt{\frac{I_{3\sigma}}{I_{2\sigma}}} \frac{d\underline{\underline{\boldsymbol{\tau}}}^{-1}}{d\underline{\underline{\boldsymbol{\sigma}}}} : \frac{d\underline{\underline{\boldsymbol{\tau}}}}{d\underline{\underline{\boldsymbol{\sigma}}}}$$

$$\frac{dr_z}{d\underline{\underline{\boldsymbol{\sigma}}}} = \left(\frac{1}{2r_z I_{2\sigma}} \frac{dI_{3\sigma}}{d\underline{\underline{\boldsymbol{\sigma}}}} - \frac{I_{3\sigma}}{2r_z I_{2\sigma}^2} \frac{dI_{2\sigma}}{d\underline{\underline{\boldsymbol{\sigma}}}} \right) \quad (71)$$

In the following, λ_k and $\underline{\underline{\mathbf{P}}}_k$ are the *eigen-vectors* and the *eigen-projectors* of $\underline{\underline{\boldsymbol{\sigma}}}$, respectively. The eigenprojectors are the three tensors formed by the dyadic between the eigenvectors as in:

$$\underline{\underline{\mathbf{P}}}_k = \underline{\underline{\mathbf{e}}}\mathbf{v}^{(k)} \otimes \underline{\underline{\mathbf{e}}}\mathbf{v}^{(k)} \quad (\text{no num on } k) \quad (72)$$

in which $\underline{\underline{\mathbf{e}}}\mathbf{v}_k$ are the eigenvectors of $\underline{\underline{\boldsymbol{\sigma}}}$ and the following expression represents the *spectral decomposition*

$$\underline{\underline{\boldsymbol{\sigma}}} = \sum_k \lambda_k \underline{\underline{\mathbf{P}}}_k \quad (k=1,2,3) \quad (73)$$

$$\frac{d\underline{\underline{\boldsymbol{\tau}}}}{d\underline{\underline{\boldsymbol{\sigma}}}} = \left(\sum_k \frac{1}{\sqrt{\lambda_k}} \underline{\underline{\mathbf{P}}}_k \bullet \underline{\underline{\boldsymbol{\sigma}}} \right) \otimes \frac{dr_z}{d\underline{\underline{\boldsymbol{\sigma}}}} \quad (74)$$

$$+ r_z \sum_k \left(\frac{1}{\sqrt{\lambda_k}} \frac{d\underline{\underline{\mathbf{C}}}_k}{d\underline{\underline{\boldsymbol{\sigma}}}} - \frac{1}{2\lambda_k^{\frac{3}{2}}} \underline{\underline{\mathbf{C}}}_k \otimes \underline{\underline{\mathbf{P}}}_k \right) \quad (75)$$

$$\underline{\underline{\mathbf{C}}}_k = \underline{\underline{\mathbf{P}}}_k \bullet \underline{\underline{\boldsymbol{\sigma}}} \quad (76)$$

$$\begin{aligned} \frac{d\underline{\underline{\mathbf{C}}}_k}{d\underline{\underline{\boldsymbol{\sigma}}}} &= \left[\underline{\underline{\boldsymbol{\sigma}}} \bullet \underline{\underline{\boldsymbol{\sigma}}} + (\lambda_k - I_{1\sigma}) \underline{\underline{\boldsymbol{\sigma}}} + \frac{I_{3\sigma}}{\lambda_k} \underline{\underline{\mathbf{I}}} \right] \\ &\otimes \left\{ \frac{1}{\alpha_k} \underline{\underline{\mathbf{P}}}_k - \frac{\lambda_k}{\alpha_k^2} \left[(6\lambda_k - 2I_{1\sigma}) \underline{\underline{\mathbf{P}}}_k + (I_{1\sigma} - 2\lambda_k) \underline{\underline{\mathbf{I}}} - \underline{\underline{\boldsymbol{\sigma}}} \right] \right\} \end{aligned} \quad (77)$$

$$\alpha_k = 2\lambda_k^2 - I_{1\sigma} \lambda_k + \frac{I_{3\sigma}}{\lambda_k} \quad (78)$$

$$\frac{d\underline{\underline{\boldsymbol{\tau}}}^{-1}}{d\underline{\underline{\boldsymbol{\tau}}}} = \frac{-1}{2} \left(\underline{\underline{\boldsymbol{\tau}}}^{-1} \otimes \underline{\underline{\boldsymbol{\tau}}}^{-1} + \underline{\underline{\boldsymbol{\tau}}}^{-1} \boxtimes \underline{\underline{\boldsymbol{\tau}}}^{-1} \right) \quad (79)$$

$$\frac{d\underline{\underline{\boldsymbol{\tau}}}}{d\underline{\underline{\boldsymbol{\sigma}}}} = \sum_k \left(\frac{1}{2\sqrt{\lambda_k}} \underline{\underline{\mathbf{P}}}_k \otimes \underline{\underline{\mathbf{P}}}_k + \sqrt{\lambda_k} \frac{d\underline{\underline{\mathbf{P}}}_k}{d\underline{\underline{\boldsymbol{\sigma}}}} \right) \quad (80)$$

$$\begin{aligned} \frac{d\underline{\underline{\mathbf{P}}}_k}{d\underline{\underline{\boldsymbol{\sigma}}}} &= \frac{\lambda_k}{\alpha_k} \left(\underline{\underline{\mathbf{I}}}^{sym} - \frac{I_{3\sigma}}{\lambda_k} \underline{\underline{\mathbf{I}}}^{\sigma^{-1}} \right) \\ &+ \frac{\lambda_k}{\alpha_k} \sum_j \left(\frac{I_{3\sigma}}{\lambda_k \lambda_j^2} - 1 \right) \underline{\underline{\mathbf{P}}}_j \otimes \underline{\underline{\mathbf{P}}}_j \end{aligned} \quad (81)$$

$$\underline{\underline{\mathbf{I}}}^{sym} = \frac{1}{2} \left(\underline{\underline{\mathbf{I}}} \otimes \underline{\underline{\mathbf{I}}} + \underline{\underline{\mathbf{I}}} \boxtimes \underline{\underline{\mathbf{I}}} \right) \quad (82)$$

$$\underline{\underline{\mathbf{I}}}^{\sigma^{-1}} = \frac{1}{2} \left(\underline{\underline{\boldsymbol{\sigma}}}^{-1} \otimes \underline{\underline{\boldsymbol{\sigma}}}^{-1} + \underline{\underline{\boldsymbol{\sigma}}}^{-1} \boxtimes \underline{\underline{\boldsymbol{\sigma}}}^{-1} \right) \quad (83)$$

$$\underline{\underline{\mathbf{N}}}_1 = \underline{\underline{\mathbf{0}}} \quad (84)$$

$$\underline{\underline{\mathbf{R}}}_1 = \left(\underline{\underline{\mathbf{I}}}^{sym} : \frac{d\underline{\underline{\boldsymbol{\tau}}}}{d\underline{\underline{\boldsymbol{\sigma}}}} - \frac{G}{t_N^2} \frac{dt_N}{d\underline{\underline{\boldsymbol{\sigma}}}} \right) \frac{t_{N1}}{\chi} \quad (85)$$

$$\underline{\underline{\mathbf{R}}}_2 = \left(\underline{\underline{\mathbf{I}}}^{sym} : \frac{d\underline{\underline{\boldsymbol{\tau}}}}{d\underline{\underline{\boldsymbol{\sigma}}}} \right) \frac{t_{N1e}}{\chi} \quad (86)$$

$$S_{11} = \frac{\text{tr}(\underline{\underline{\mathbf{r}}})}{\chi} + \frac{G - k}{t_{N\chi}} \quad (87)$$

$$S_{12} = \frac{t_{N1k}}{t_{N1e} t_{N\chi}} \quad (88)$$

$$S_{21} = 0 \quad (89)$$

$$S_{22} = \frac{\text{tr}(\underline{\underline{\mathbf{r}}})}{\chi} \quad (90)$$